Supporting Information for

Thermodynamic Modeling Suggests Declines in Water Uptake and Acidity of Inorganic Aerosols in Beijing Winter Haze Events during 2014/2015–2018/2019

Shaojie Song,[†,‡] Athanasios Nenes,[§,£] Meng Gao,[‡] Yuzhong Zhang,[‡] Pengfei Liu,[‡] Jingyuan Shao,[⊥] Dechao Ye,[†] Weiqi Xu,[#] Lu Lei,[#] Yele Sun,[#,*] Baoxian Liu,[†,Ⅱ,*] Shuxiao Wang,[†,×*] Michael B. McElroy[‡]

[†]School of Environment, State Key Joint Laboratory of Environment Simulation and Pollution Control, Tsinghua University, Beijing 100084, China

[‡]School of Engineering and Applied Sciences, Harvard University, Cambridge, Massachusetts 02138, USA

[§]School of Architecture, Civil and Environmental Engineering, Ecole Polytechnique Fédérale de Lausanne, CH-1015, Lausanne, Switzerland

[£]Institute for Chemical Engineering Sciences, Foundation for Research and Technology Hellas, Patras, GR-26504, Greece

[⊥]School of Physics, Peking University, Beijing 100871, China

[#]State Key Laboratory of Atmospheric Boundary Physics and Atmospheric Chemistry, Institute of Atmospheric Physics, Chinese Academy of Sciences, Beijing 100029, China

[Ⅱ]Beijing Key Laboratory of Airborne Particulate Matter Monitoring Technology, Beijing Municipal Environmental Monitoring Center, Beijing 100048, China

[×]State Environmental Protection Key Laboratory of Sources and Control of Air Pollution Complex, Beijing 100084, China

Corresponding to:

S.W. (E-mail: shxwang@tsinghua.edu.cn), Y.S. (E-mail: sunyele@mail.iap.ac.cn), and B.L. (E-mail: liubaoxian28@163.com)

S1. Details of Field Measurements

Sampling periods for the four winter seasons (defined by the heating period from 15th November to 15th March) campaigns were (format of date: YYYY.MM.DD) 2014.11.17–2015.01.18, 2016.11.23–2016.12.14, 2017.11.15–2017.12.31, and 2018.11.20–2018.12.25, respectively. A small proportion of measurement data was missing or removed due to snow events and instrument failure. Meteorological variables and aerosol chemical species were measured at a ground-based site in the Institute of Atmospheric Physics, Chinese Academy of Sciences (39.976N 116.378E), and gaseous ammonia was measured at the Beijing municipal environmental protection monitoring iencies using pure ammonium nitrate particles were performed following the standard procedures. ADDIN EN.C

RH and *T* were recorded using a Rotronic HC2-S3 probe. The overall absolute uncertainties for the measured RH and *T* were estimated according to instrumental precisions, i.e., 0.1 °C and 1.0 %, respectively.

Non-refractory submicron particles (NR-PM_1) chemical species during three winter seasons (2014/2015, 2016/2017, and 2018/2019) were measured with the same high-resolution time-of-flight aerosol mass spectrometer (HR-ToF-AMS; Aerodyne Research Inc., USA). As described in our previous papers,[1,2] the collected mass spectrometer data were analyzed using the standard software packages. A default collection efficiency of 0.5 was used, because the mass fractions of ammonium nitrate were below 45%,[3] the aerosols were expected to be moderately acidic,[4] and the silica gel dryers reduced RH in the sampling line. The calibrations of ionization efficiencies using pure ammonium nitrate particles were performed following the standard procedures.[5,6] The overall relative uncertainties for the concentrations of aerosol chemical components (ammonium (35%), nitrate (33%), sulfate (36%), and chloride (40%)) were estimated based on a previous study.[7] They

were mainly contributed by errors in collection efficiency but also by other factors, including the uncertainties in nitrate ionization efficiency, flow rates, transmission efficiency, and ionization efficiency of a certain species relative to nitrate (also known as RIE_{NO3}).[7] It was noted, although the nitrate mass fraction increased from 14% to 35% from 2014/2015 winter to 2018/2019 winter (see Figure 1 in the main text), that the collection efficiency did not change significantly. This was because the mass fraction of ammonium nitrate was still less than 45% under which conditions the collection efficiency was insensitive to its variation.[3] Different from the uncertainties for the mass concentrations, the uncertainties for the mass fractions of different chemical species only depended on RIE_{NO3}, which was about 10% for ammonium and 15% for sulfate.

The NR-PM_1 chemical species for 2017/2018 winter were measured by an aerosol chemical speciation monitor (ACSM) that was also developed by Aerodyne Research Inc. Intercomparison experiments between HR-ToF-AMS and ACSM showed that all the species were well correlated ($R^2 > 0.9$) whereas the slopes of different species were different from 1.0 (ranging from 0.6 to 1.2). The different slopes between ACSM and HR-ToF-AMS were due in part to the resolutions of mass spectrometry and the fragmentation tables.[8] Thus, in order to remove the systematic errors among different winter seasons, the data collected by the ACSM were corrected using the scaling factors identified from the intercomparison experiments against HR-ToF-AMS.

For the four winter seasons (from 2014/2015 to 2018/2019), gaseous ammonia was measured by the same chemiluminescent analyzer (model 17i, Thermo Fisher Scientific Inc., USA), and the lower detection limit and precision were about 1 ppb. Standard gas was used for calibration every two weeks and filter membrane was replaced every week. The overall relative uncertainty of 30% was estimated from the available intercomparison studies.[9-11]

As described in the main text, all the model inputs (including *T*, RH, and gaseous and aerosol chemical species) were averaged on an hourly basis for thermodynamic calculations. The Monte Carlo approach was used to propagate the uncertainties within measurements to model predictions. All input variables were assumed to follow a uniform distribution and their values were selected randomly and calculated 1000 times for each hourly sample. Since the same instrument was used for a certain type of measurements, systematic errors during different winters were unexpected, and thus the overall uncertainties described above were assumed to be random errors. It was noted that the systematic errors between ACSM and HR-ToF-AMS have been removed, as mentioned earlier in this section.

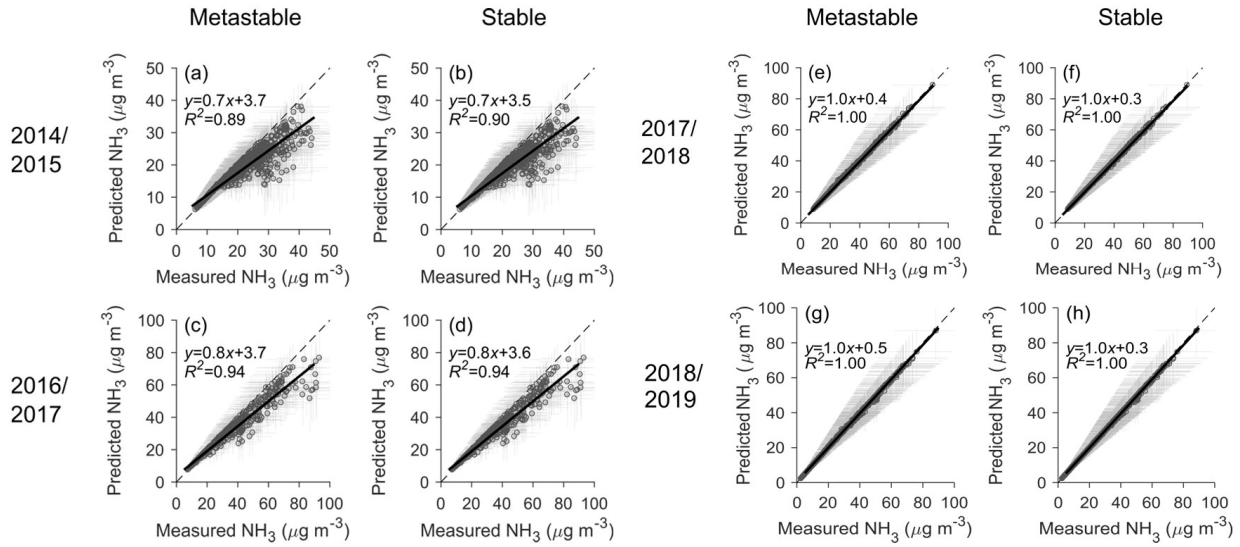

Figure S1. Comparison of measured and ISORROPIA predicted gaseous NH_3 concentrations for the investigated four winter seasons (2014/2015, 2016/2017, 2017/2018, and 2018/2019). (a), (c), (e), and (g) show calculations derived using the metastable assumption, whereas (b), (d), (f), and (h) show results obtained with the stable assumption.

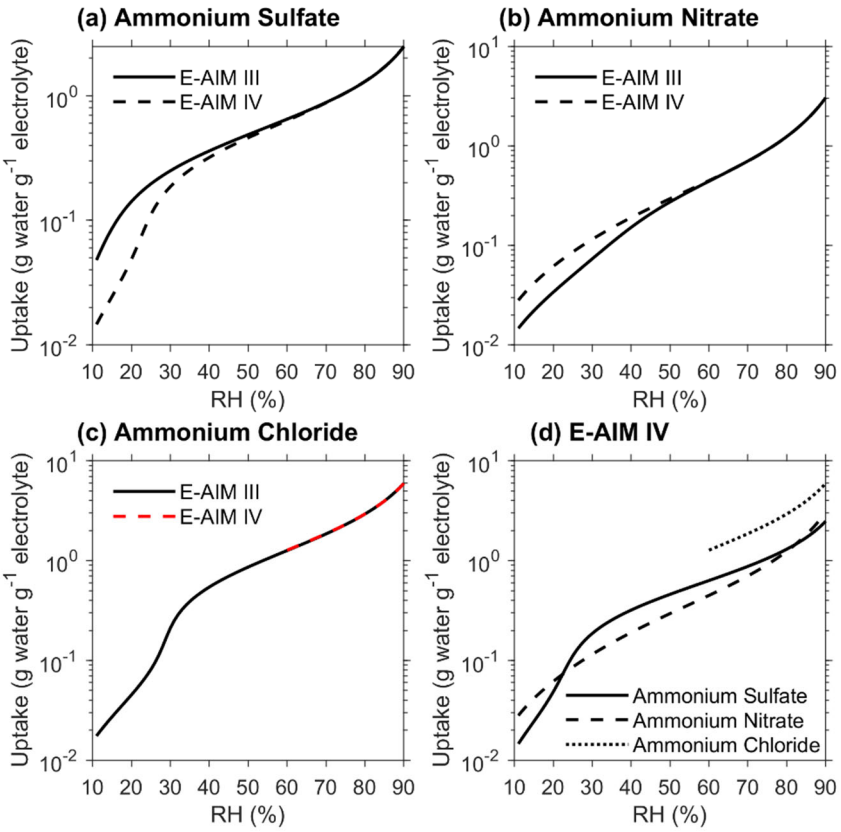

Figure S2. (a–c) are comparisons of the amount of water uptake per mass of different electrolytes (ammonium sulfate, ammonium nitrate, and ammonium chloride). Data are obtained from E-AIM III and IV. (d) is a summary of E-AIM IV data for the three electrolytes.

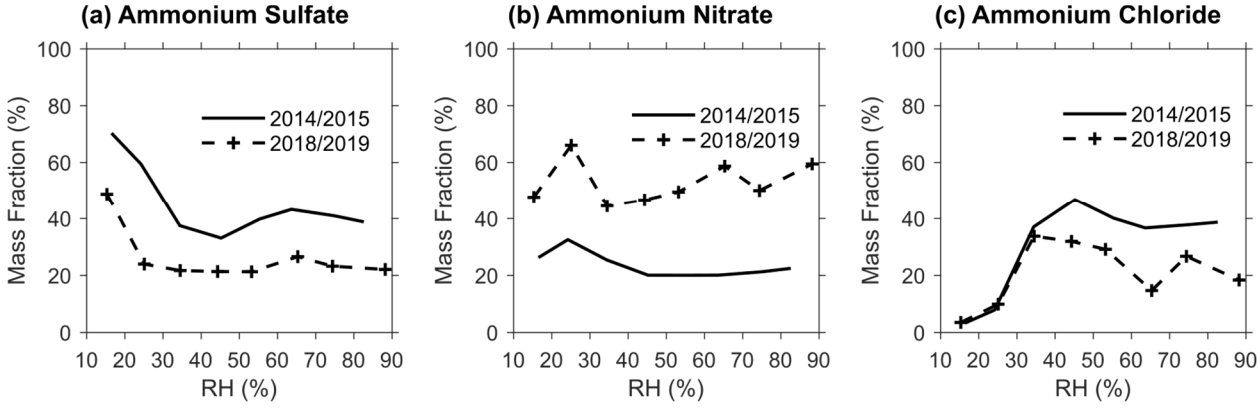

Figure S3. Mass fractions of aerosol water content associated with different electrolytes (a–c are ammonium sulfate, ammonium nitrate, and ammonium chloride, respectively). Data for two winter seasons (2014/2015 and 2018/2019) are re-calculated using the water-uptake data from E-AIM IV. Data are grouped in RH bins (10% increment).

S2. Buffer Equation Derived from Partitioning of Ammonia

For the acid/base gas–aerosol system in Beijing winter haze that is buffered by the partitioning of semivolatile ammonia, the relevant equilibrium relations (①, ②, and ③) and their constants are shown in Table S1.

Table S1. Equilibrium relations and constants. Constants are obtained from ref.[12].

	Equilibrium relation	Constant expression	Equilibrium constant			Unit
			$K(T_0)$	a	b	
①	$NH_{3(g)} \leftrightarrow NH_{3(aq)}$	$K_1 = \frac{[NH_{3(aq)}]}{P_{NH_{3(g)}}} \gamma_{NH_{3(aq)}}$	57.64	13.79	−5.39	mol kg^{-1} atm^{-1}
②	$NH_{3(aq)} + H_2O_{(aq)} \leftrightarrow NH_{4(aq)}^+ + OH_{(aq)}^-$	$K_2 = \frac{[NH_{4(aq)}^+][OH_{(aq)}^-]}{[NH_{3(aq)}]a_w} \frac{\gamma_{NH_{4(aq)}^+}\gamma_{OH_{(aq)}^-}}{\gamma_{NH_{3(aq)}}}$	1.805×10^{-5}	−1.50	26.92	mol kg^{-1}
③	$H_2O_{(aq)} \leftrightarrow H_{(aq)}^+ + OH_{(aq)}^-$	$K_3 = \frac{[H_{(aq)}^+][OH_{(aq)}^-]}{a_w} \gamma_{H_{(aq)}^+}\gamma_{OH_{(aq)}^-}$	1.01×10^{-14}	−22.52	26.92	mol^2 kg^{-2}

$T_0 = 298$ K and $K = K(T_0)\exp\left[a\left(\frac{T_0}{T} - 1\right) + b\left(1 + \ln\left(\frac{T_0}{T}\right) - \frac{T_0}{T}\right)\right]$.

① + ② − ③ gives

$$NH_{3(g)} + H_{(aq)}^+ \leftrightarrow NH_{4(aq)}^+ \qquad ④$$

The equilibrium constant K_4 (unit: atm^{-1}) is given by

$$K_4 = \frac{[NH_{4(aq)}^+]\gamma_{NH_{4(aq)}^+}}{P_{NH_{3(g)}}[H_{(aq)}^+]\gamma_{H_{(aq)}^+}} = \frac{K_1K_2}{K_3}$$

Rearrangement of this expression and taking logarithms yields

$$pH = -\log_{10}\left([H_{(aq)}^+]\gamma_{H_{(aq)}^+}\right) = -\log_{10}\left(\frac{[NH_{4(aq)}^+]\gamma_{NH_{4(aq)}^+}}{P_{NH_{3(g)}}K_4}\right)$$

Combining the above equation and the general gas equation $P_{NH_{3(g)}} = [NH_{3(g)}]RT$ gives

$$pH = -\log_{10}\left(\frac{[NH_{4(aq)}^{+}]\gamma_{NH_{4(aq)}^{+}}}{[NH_{3(g)}]RTK_4}\right)$$

where $[NH_{3(g)}]$ represents the molar concentration of $NH_{3(g)}$ (μmol m^{-3}) and R is the gas constant (= 8.206×10^{-11} m^3 atm K^{-1} μmol^{-1}).

Rearrangement of this expression gives

$$pH = pK^{*} + \log_{10}\left(\frac{[NH_{3(g)}]}{a_{NH_{4(aq)}^{+}}}\right) \quad ⑤$$

where $K^{*}(\mu mol\ m^{-3}) = K_3/(RTK_1K_2)$ represents the apparent equilibrium constant, $[NH_{3(g)}]$ (μmol m^{-3}) represents the molar concentration of gaseous ammonia, and $a_{NH_{4(aq)}^{+}}(mol\ kg^{-1}) = [NH_{4(aq)}^{+}]\gamma_{NH_{4(aq)}^{+}}$ represents the molality-based activity of $NH_{4(aq)}^{+}$.

Equation ⑤ serves as the buffer equation for the gas–aerosol system controlled by partitioning of ammonia. Its format is identical to that of the Henderson–Hasselbalch equation (for a monobasic acid $HA \leftrightarrow H^{+} + A^{-}$, $pH = pK_a + \log_{10}\left(\frac{[A^{-}]}{[HA]}\right)$, where K_a is the acid dissociation constant), which can be used to estimate the pH of a buffer solution containing given concentrations of an acid and its conjugate base (or a base and its conjugate acid). It should be noted, unlike the Henderson–Hasselbalch equation, in Equation ⑤ that the numerator ($[NH_{3(g)}]$) and denominator ($a_{NH_{4(aq)}^{+}}$) have different units and that pK^{*} does not have the unit with pH.

The buffer equation ⑤ for aerosol pH, which contains three variables, pK^{*}, $[NH_{3(g)}]$, and $a_{NH_{4(aq)}^{+}}$, can help conceptually understand the meteorological and chemical factors that influence

pH. The first term on the right-hand side, pK^*, is only a function of temperature, and as shown in Figure S4a, decreases by about 0.05 unit with one Kelvin increase in temperature. This dependence reflects both changes in Equations ① (solubility of ammonia) and ③ (dissociation of water). The second term on the right-hand side, $\log_{10}\left(\frac{[NH_{3(g)}]}{a_{NH_{4(aq)}^+}}\right)$, reflects the effect of NH_x partitioning on pH. A 10-fold increase in $[NH_{3(g)}]$ corresponds to a one unit increase in pH.[13] $a_{NH_{4(aq)}^+}$ is influenced by both the water activity (a_w, or RH) and the aerosol chemical composition (other ions coexisting in the particle phase).

Next, we use three sensitivity calculations to show that the simple buffer equation ⑤ can help understand pH results obtained from full thermodynamic equilibrium models. Recall that equation ⑤ contains three variables pK^* (only a function of temperature T), $[NH_{3(g)}]$, and $a_{NH_{4(aq)}^+}$ (affected by both RH and aerosol chemical composition). The three sensitivity calculations are designed to evaluate the influences of these three factors separately. Overall, these sensitivity calculations demonstrate that the buffer equation can well describe the influence of different factors (T, $[NH_{3(g)}]$, and $a_{NH_{4(aq)}^+}$) on the calculated pH values from full thermodynamic equilibrium models, suggesting its ability to help conceptually understand aerosol pH.

The first sensitivity test investigates the influence of T on aerosol pH. To isolate the influence of T, we specify the model inputs: RH (= 70%), $[NH_{3(g)}]$ (= 1.0 μmol m^{-3}), $[NH_{4(aq)}^+]$ (= 1.0 μmol m^{-3}), $[SO_{4(aq)}^{2-}]$ (= 0.24 μmol m^{-3}), $[NO_{3(aq)}^-]$ (= 0.24 μmol m^{-3}), $[Cl_{(aq)}^-]$ (= 0.28 μmol m^{-3}), and vary T from 270 K to 300 K. The relative contributions of $SO_{4(aq)}^{2-}$, $NO_{3(aq)}^-$, and $Cl_{(aq)}^-$ are estimated from the average winter haze conditions in 2014/2015 (Figure 1 in the main text). Note in this study that we always use the so-called forward mode in thermodynamic model calculations, whose

model inputs are the total (gas + aerosol) chemical measurements. For example, in this sensitivity test, the total NH_x (= $[NH_{3(g)}] + [NH_{4(aq)}^+]$) in the gas–aerosol equilibrium system is 2.0 μmol m^{-3}, the total H_2SO_4 (= $[SO_{4(aq)}^{2-}] + [H_2SO_{4(g)}]$) is 0.24 μmol m^{-3}, the total HNO_3 (= $[NO_{3(aq)}^-] + [HNO_{3(g)}]$) is 0.24 μmol m^{-3}, and the total HCl (= $[Cl_{(aq)}^-] + [HCl_{(g)}]$) is 0.28 μmol m^{-3}. Based on these input data in the total aerosol–gas system, the thermodynamic models (ISORROPIA and E-AIM) calculate the phase partitioning of these acid and basic species at chemical equilibrium.

As shown in Figure S4a, pK^* is almost a linear function of T and the slope $\frac{\partial pK^*}{\partial T} = -0.054$. Since RH, $[NH_{3(g)}]$, and $[NH_{4(aq)}^+]$ remain constants in this test, the buffer equation suggests that $\frac{\partial pH}{\partial T} \approx \frac{\partial pK^*}{\partial T} = -0.054$. Figures S4b and S4c show the relationships between the modeled pH and T from ISORROPIA and E-AIM, respectively. Like the suggestions from the buffer equation ⑤, these full thermodynamic modeling analyses show nearly linear correlations (R^2 = 1.0) between pH and T, and the modeled slopes $\frac{\partial pH}{\partial T}$ are −0.045 and −0.056, respectively, comparing well with $\frac{\partial pH}{\partial T} \approx -0.054$ obtained from the buffer equation ⑤.

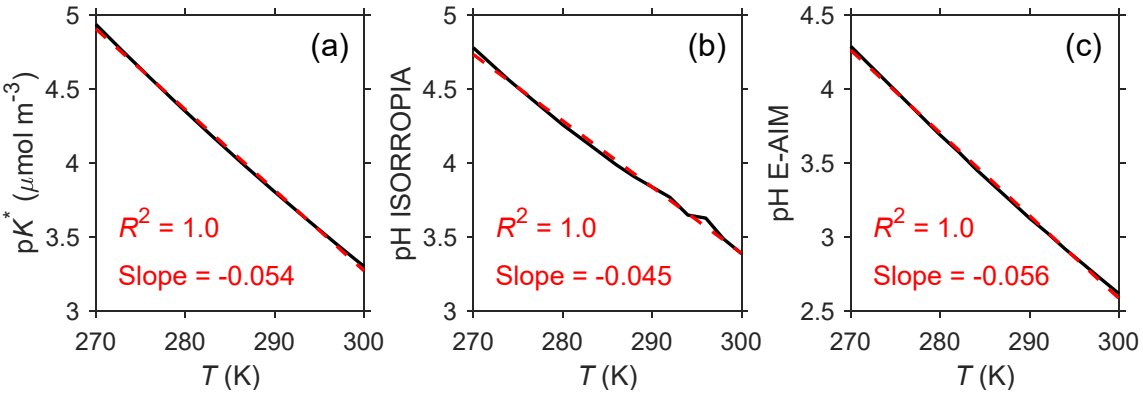

Figure S4. Results from the first sensitivity test. Panel (a) shows the dependence of pK^* on T. Panels (b) and (c) show relationships between pH calculated from ISORROPIA and E-AIM, respectively, and T. The slopes and R^2 are calculated from linear regression fits.

The second sensitivity test investigates the influence of $[NH_{3(g)}]$ on aerosol pH. To isolate the influence of $[NH_{3(g)}]$, we specify the model inputs: T (= 278 K), RH (= 70%), $[NH^{+}_{4(aq)}]$ (= 1.0 μmol m^{-3}), $[SO^{2-}_{4(aq)}]$ (= 0.24 μmol m^{-3}), $[NO^{-}_{3(aq)}]$ (= 0.24 μmol m^{-3}), $[Cl^{-}_{(aq)}]$ (= 0.28 μmol m^{-3}), and vary $[NH_{3(g)}]$ from 0.1 μmol m^{-3} to 5 μmol m^{-3}. The relative contributions of $SO^{2-}_{4(aq)}$, $NO^{-}_{3(aq)}$, and $Cl^{-}_{(aq)}$ are estimated from the average winter haze conditions in 2014/2015 (Figure 1 in the main text). Since T, RH, and $[NH^{+}_{4(aq)}]$ remain constants in this test, the buffer equation ⑤ suggests that $\frac{\partial pH}{\partial \log_{10}([NH_{3(g)}])} = 1$. As shown in Figure S5, pH calculated from both ISORROPIA (panel a) and E-AIM (panel b) show perfect (R^2 = 1.0) linear correlations with $\log_{10}([NH_{3(g)}])$ and the slopes $\frac{\partial pH}{\partial \log_{10}([NH_{3(g)}])} = 1.0$.

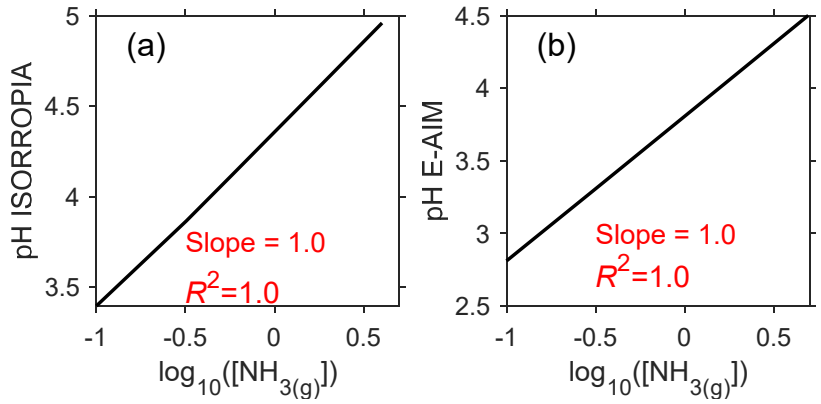

Figure S5. Results from the second sensitivity test. Panels (a) and (b) show relationships between pH calculated from ISORROPIA and E-AIM, respectively, and $\log_{10}([NH_{3(g)}])$. The slopes and R^2 are calculated from linear regression fits.

The third sensitivity test investigates the influence of $a_{NH^{+}_{4(aq)}}$ on aerosol pH. Since $a_{NH^{+}_{4(aq)}}$ is affected by both RH and aerosol chemical composition, we specify the model inputs: T (= 278 K), $[NH_{3(g)}]$ (= 1.0 μmol m^{-3}), $[NH^{+}_{4(aq)}]$ (= 1.0 μmol m^{-3}), and vary RH from 60% to 90%. We also

specify the relative contributions of $SO_{4(aq)}^{2-}$, $NO_{3(aq)}^{-}$, and $Cl_{(aq)}^{-}$ from the average haze conditions in different winter seasons (from 2014/2015 to 2018/2019 following Figure 1 in the main text). Since T and $[NH_{3(g)}]$ remain constants in this test, the buffer equation ⑤ suggests that $\triangle \text{pH} = -\triangle \log_{10}\left(a_{NH_{4(aq)}^{+}}\right) = -\triangle \log_{10}\left([NH_{4(aq)}^{+}]\gamma_{NH_{4(aq)}^{+}}\right)$. Thus, we expect, for a specific season, with increases in RH, that $[NH_{4(aq)}^{+}]$ (molality) decreases (due to higher aerosol water uptake) and pH increases (supposing $\gamma_{NH_{4(aq)}^{+}}$ does not strongly vary with RH). The E-AIM model results, as shown in Figure S6, are consistent with insights from the buffer equation. With increases in RH, $a_{NH_{4(aq)}^{+}}$ decreases, pH increases, and $-\log_{10}\left(a_{NH_{4(aq)}^{+}}\right)$ and pH have a perfect linear relationship (slope = 1.0, R^2 = 1.0). Figure S6 also shows that the temporal change in aerosol composition (more nitrate and less sulfate and chloride) from 2014/2015 to 2018/2019 decreases $\log_{10}\left(a_{NH_{4(aq)}^{+}}\right)$ (due to the change in $\gamma_{NH_{4(aq)}^{+}}$) and thus increases aerosol pH (by about 0.1 unit at 80% RH).

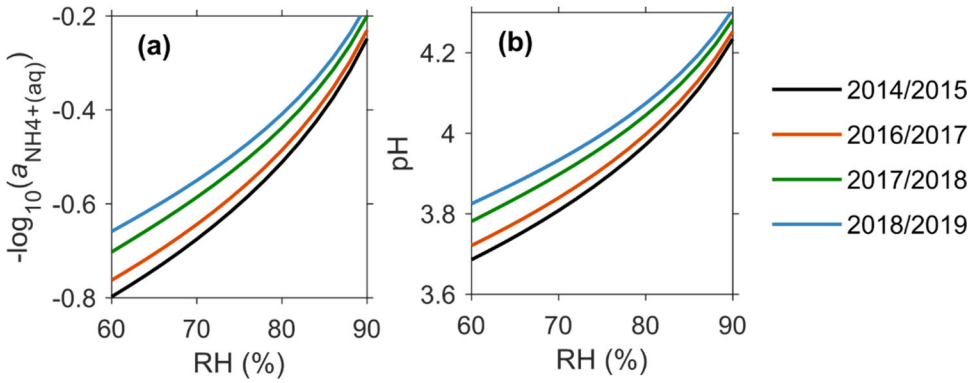

Figure S6. Results from the third sensitivity test. Relationships are shown between RH and $-\log_{10}\left(a_{NH_{4(aq)}^{+}}\right)$ (a), and between RH and pH (b). In the sensitivity test, the molar concentrations of anions are $[SO_{4(aq)}^{2-}]$ (= 0.24 μmol m^{-3}), $[NO_{3(aq)}^{-}]$ (= 0.24 μmol m^{-3}), $[Cl_{(aq)}^{-}]$ (= 0.28 μmol m^{-3}) in 2014/2015, $[SO_{4(aq)}^{2-}]$ (= 0.23 μmol m^{-3}), $[NO_{3(aq)}^{-}]$ (= 0.32 μmol m^{-3}), $[Cl_{(aq)}^{-}]$ (= 0.23 μmol m^{-3}) in 2016/2017, are $[SO_{4(aq)}^{2-}]$ (= 0.21 μmol m^{-3}), $[NO_{3(aq)}^{-}]$ (= 0.46 μmol m^{-3}), $[Cl_{(aq)}^{-}]$ (= 0.12 μmol

m^{-3}) in 2017/2018, and are $\left[SO_{4(aq)}^{2-}\right]$ (= 0.14 μmol m^{-3}), $\left[NO_{3(aq)}^{-}\right]$ (= 0.58 μmol m^{-3}), $\left[Cl_{(aq)}^{-}\right]$ (= 0.14 μmol m^{-3}) in 2018/2019. The relative contributions of these species are specified according to the average haze conditions in different winter seasons (Figure 1 in the main text).

S3. Influence of Nonvolatile Cations and Hydrophilic Organic Acids

In order to evaluate the potential influence of minor water-soluble aerosol species (nonvolatile cations and hydrophilic organic acids that were not available in our measurements) on aerosol acidity and water uptake, we conducted two sensitivity calculations using thermodynamic models and the data measured by other studies under Beijing winter haze conditions. Results from these model calculations suggested that considering these minor water-soluble species was unlikely to alter the findings of declined aerosol acidity and water uptake.

The first one was focused on nonvolatile cations (NVCs). The mass fraction of NVCs in PM_1 was reported by Ding et al.[14] to be 7% of that of major inorganic species (the sum of ammonium, nitrate, sulfate, and chloride) at Beijing winter polluted conditions. The low contribution of NVCs was attributed to the low wind speeds associated with haze conditions and to the size distribution of dust species (primarily residing in the coarse mode). One conclusion of this study was that the inorganic aerosol pH increased by 0.3–0.4 unit from winter 2014/2015 to 2018/2019. Thus, this sensitivity calculation investigated the influence of NVCs on aerosol pH for 2014/2015. Results from ISORROPIA showed that including NVCs (using Na^+ as the representative) could increase the modeled pH by about 0.12 unit for 2014/2015, which was minor compared with the pH increase of 0.3–0.4 unit from 2014/2015 to 2018/2019. Results also showed a minor (~ 2%) influence of NVCs on the modeled aerosol mass growth factor G_{mi}.

The second was focused on hydrophilic organic acids. Recent work by Wang et al.[15,16] showed that oxalate, one of the strongest organic acids (acid dissociation constants $pK_{a1} = 1.27$ and $pK_{a2} = 4.27$), was the major organic acid salt species in Beijing winter haze aerosols and its concentration was about 1–2% of the sulfate concentration. Earlier studies[17,18] showed that oxalate accounted about a half for the detected organic acid species. Therefore, we conducted a sensitivity calculation

using ISORROPIA by including oxalate equal to 4% of the measured aerosol sulfate for 2014/2015. Results from the E-AIM calculation showed that the changes in the modeled aerosol pH and mass growth factor were < 0.02 unit and < 1%, respectively.

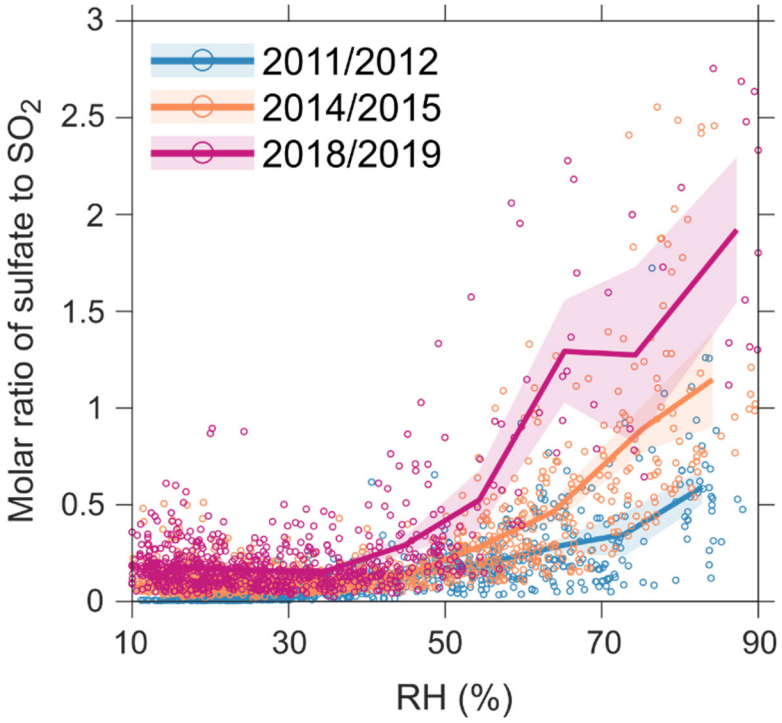

Figure S7. Observed relationship between sulfate/SO_2 molar ratio and RH for three winter seasons (2011/2012, 2014/2015, and 2018/2019). The circles indicate hourly observations. The lines and shaded regions indicate the mean values and their 95% confidence intervals (calculated as $\overline{X} \pm Z\frac{S}{\sqrt{n}}$ where $\overline{X}$ was the mean, Z was the Z-value and equal to 1.96, S was the standard deviation, and n was the number of hourly observations) which were grouped in RH bins (10% increment). Data in 2011/2012 winter (from 21 November 2011 to 20 January 2012) were obtained from Sun et al. (2013)[1], which were also collected at the ground-based site in the Institute of Atmospheric Physics, Chinese Academy of Sciences (39.976N, 116.378E). The SO_2 data in 2014/2015 and 2018/2019 winter seasons were measured by Beijing municipal environmental monitoring center (*http://www.bjmemc.com.cn*) at the routine station Chao-Yang-Ao-Ti-Center (39.982N, 116.397E; about 2 km away from Institute of Atmospheric Physics).

References

(1) Sun, Y.; Wang, Z.; Fu, P.; Jiang, Q.; Yang, T.; Li, J.; Ge, X. The impact of relative humidity on aerosol composition and evolution processes during wintertime in Beijing, China. *Atmos. Environ.* **2013,** *77*, 927-934.
(2) Xu, W.; Sun, Y.; Wang, Q.; Zhao, J.; Wang, J.; Ge, X.; Xie, C.; Zhou, W.; Du, W.; Li, J.; Fu, P.; Wang, Z.; Worsnop, D. R.; Coe, H. Changes in aerosol chemistry from 2014 to 2016 in winter in Beijing: Insights from high-resolution aerosol mass spectrometry. *J. Geophys. Res. Atmos.* **2019,** *124*, 1132-1147.
(3) Middlebrook, A. M.; Bahreini, R.; Jimenez, J. L.; Canagaratna, M. R. Evaluation of Composition-Dependent Collection Efficiencies for the Aerodyne Aerosol Mass Spectrometer using Field Data. *Aerosol Science and Technology* **2012,** *46*, 258-271.
(4) Song, S.; Gao, M.; Xu, W.; Shao, J.; Shi, G.; Wang, S.; Wang, Y.; Sun, Y.; McElroy, M. B. Fine-particle pH for Beijing winter haze as inferred from different thermodynamic equilibrium models. *Atmos. Chem. Phys.* **2018,** *18*, 7423-7438.
(5) Jayne, J. T.; Leard, D. C.; Zhang, X.; Davidovits, P.; Smith, K. A.; Kolb, C. E.; Worsnop, D. R. Development of an Aerosol Mass Spectrometer for Size and Composition Analysis of Submicron Particles. *Aerosol Science and Technology* **2000,** *33*, 49-70.
(6) Ng, N. L.; Herndon, S. C.; Trimborn, A.; Canagaratna, M. R.; Croteau, P. L.; Onasch, T. B.; Sueper, D.; Worsnop, D. R.; Zhang, Q.; Sun, Y. L.; Jayne, J. T. An Aerosol Chemical Speciation Monitor (ACSM) for Routine Monitoring of the Composition and Mass Concentrations of Ambient Aerosol. *Aerosol Science and Technology* **2011,** *45*, 780-794.
(7) Bahreini, R.; Ervens, B.; Middlebrook, A. M.; Warneke, C.; de Gouw, J. A.; DeCarlo, P. F.; Jimenez, J. L.; Brock, C. A.; Neuman, J. A.; Ryerson, T. B.; Stark, H.; Atlas, E.; Brioude, J.; Fried, A.; Holloway, J. S.; Peischl, J.; Richter, D.; Walega, J.; Weibring, P.; Wollny, A. G.; Fehsenfeld, F. C. Organic aerosol formation in urban and industrial plumes near Houston and Dallas, Texas. *J. Geophys. Res. Atmos.* **2009,** *114*.
(8) Sun, Y.; Du, W.; Wang, Q.; Zhang, Q.; Chen, C.; Chen, Y.; Chen, Z.; Fu, P.; Wang, Z.; Gao, Z.; Worsnop, D. R. Real-Time Characterization of Aerosol Particle Composition above the Urban Canopy in Beijing: Insights into the Interactions between the Atmospheric Boundary Layer and Aerosol Chemistry. *Environmental Science & Technology* **2015,** *49*, 11340-11347.
(9) Ellis, R. A.; Murphy, J. G.; Pattey, E.; van Haarlem, R.; O'Brien, J. M.; Herndon, S. C. Characterizing a Quantum Cascade Tunable Infrared Laser Differential Absorption Spectrometer (QC-TILDAS) for measurements of atmospheric ammonia. *Atmos. Meas. Tech.* **2010,** *3*, 397-406.
(10) Fehsenfeld, F. C.; Huey, L. G.; Leibrock, E.; Dissly, R.; Williams, E.; Ryerson, T. B.; Norton, R.; Sueper, D. T.; Hartsell, B. Results from an informal intercomparison of ammonia measurement techniques. *J. Geophys. Res. Atmos.* **2002,** *107*.
(11) Mennen, M. G.; Van Elzakker, B. G.; Van Putten, E. M.; Uiterwijk, J. W.; Regts, T. A.; Van Hellemond, J.; Wyers, G. P.; Otjes, R. P.; Verhage, A. J. L.; Wouters, L. W.; Heffels, C. J. G.; Romer, F. G.; Van Den Beld, L.; Tetteroo, J. E. H. Evaluation of automatic ammonia monitors for application in an air quality monitoring network. *Atmos. Environ.* **1996,** *30*, 3239-3256.
(12) Fountoukis, C.; Nenes, A. ISORROPIA II: a computationally efficient thermodynamic equilibrium model for K^+-Ca^{2+}-Mg^{2+}-NH_4^+-Na^+-SO_4^{2-}-NO_3^--Cl^--H_2O aerosols. *Atmos. Chem. Phys.* **2007,** *7*, 4639-4659.
(13) Guo, H.; Weber, R. J.; Nenes, A. High levels of ammonia do not raise fine particle pH sufficiently to yield nitrogen oxide-dominated sulfate production. *Sci. Rep.* **2017,** *7*, 12109.
(14) Ding, J.; Zhao, P.; Su, J.; Dong, Q.; Du, X.; Zhang, Y. Aerosol pH and its driving factors in Beijing. *Atmos. Chem. Phys.* **2019,** *19*, 7939-7954.
(15) Wang, G.; Zhang, F.; Peng, J.; Duan, L.; Ji, Y.; Marrero-Ortiz, W.; Wang, J.; Li, J.; Wu, C.; Cao, C.; Wang, Y.; Zheng, J.; Secrest, J.; Li, Y.; Wang, Y.; Li, H.; Li, N.; Zhang, R. Particle acidity and sulfate production during severe haze events in China cannot be reliably inferred by assuming a mixture of inorganic salts. *Atmos. Chem. Phys.* **2018,** *18*, 10123-10132.
(16) Wang, J.; Wang, G.; Gao, J.; Wang, H.; Ren, Y.; Li, J.; Zhou, B.; Wu, C.; Zhang, L.; Wang, S.; Chai, F. Concentrations and stable carbon isotope compositions of oxalic acid and related SOA in Beijing before, during, and after the 2014 APEC. *Atmos. Chem. Phys.* **2017,** *17*, 981-992.
(17) Huang, X.-F.; Hu, M.; He, L.-Y.; Tang, X.-Y. Chemical characterization of water-soluble organic acids in PM2.5 in Beijing, China. *Atmospheric Environment* **2005,** *39*, 2819-2827.
(18) Wang, Y.; Zhuang, G.; Chen, S.; An, Z.; Zheng, A. Characteristics and sources of formic, acetic and oxalic acids in PM2.5 and PM10 aerosols in Beijing, China. *Atmospheric Research* **2007,** *84*, 169-181.